environments. Figure 8A shows the amplitude and Figure 8B shows the phase. The measured field distribution is similar to the simulation results in Figure 7.

The simulated and measured field distributions are both vortex shaped. A vortex-shaped field distribution is characteristic of the OAM phenomenon.

4 | CONCLUSIONS

This article presented a novel antenna design procedure for generating the OAM phenomenon. The difference between this and other papers is that the antenna proposed here is a one-layer array antenna with an expandable structure. This design procedure is advantageous for antenna applications with large arrays and narrow beamwidths. The proposed antenna is arranged in a circular array with an 8×2 patch at an operating frequency of 5 GHz. The circular feed network at the center is designed for phase shifting and to divide the power. To generate the OAM phenomenon, a circular feed network is designed to phase shift the power divider, supplying a 45° phase difference between two neighboring feedlines (Figure 2). This produces the OAM phenomenon. At 5 GHz, the OAM phenomenon was observed in the simulations and measurements. The proposed antenna should increase the channel data capacity. Therefore, this technique is expected to be utilized in communication systems.

ACKNOWLEDGMENTS

This research was supported by a grant of the Research on Evaluation of Radio Frequency through Approach of Electromagnetic Engineering fund from RRA (Radio Research Agency) in 2017, and this research was supported by research fund from Chosun University in Korea, 2017.

REFERENCES

[1] Allen L, Beijersbergen MW, Spreeuw RJC, Woerdman JP. Orbital angular momentum of light and the transformation of Laguerre-Gaussian laser modes. *Phys Rev A.* 1992;45:8185–8189.

[2] GibsonCourtial GJ, Padgett M, Vasnetsov J, Pasko MV, Barnett SM, Franke-Arnold S. *Free-Space Information Transfer Using Light Beams Carrying Orbital Angular Momentum*. Optics Express; 2004.

[3] Sjoholm J, Palmer K, Thide B. Angular Momentum of Electromagnetic Radiation [Diploma Thesis]. Uppsala University; 2007.

[4] Tan Y, Li L, Ruan H. An efficient approach to generate microwave vector-vortex fields based on metasurface. *Microwave Opt Technol Lett.* 2015;57:1708–1713.

[5] Guo H, Wang Y, Li X, Zhang L, Fang Y, Chi N. 75GBAUD NYQUIST QPSK signal transmission with orbital angular momentum multiplexing. *Microwave Opt Technol Lett.* 2016;58:1866–1869.

[6] Edfors O, Johansson AJ. Is orbital angular momentum (OAM) based radio communications and unexploited area? *IEEE Trans Antennas Propag.* 2012;60:1126–1131.

[7] TamburiniMari F, Sponselli E, Thide A, Bianchini BA, Romanato F. Encoding many channels on the same frequency through radio vorticity: first experimental test. *New J Phys.* 2012;14.

[8] Mohammadi SM, Daldorff L, Bergman J, et al. Orbital angular momentum in radio – a system study. *IEEE Trans Antennas Propag.* 2010;58:565–572.

[9] ThidéThen B, Sjöholm H, Palmer J, et al. Utilization of photon orbital angular momentum in the low-frequency radio domain. *Phys Rev Lett.* 2007;99:087701.

[10] YuLi S, Shi L, Zhu G, Zhou CX, Shi Y. Design, fabrication, and measurement of reflective metasurface for orbital angular momentum vortex wave in radio frequency domain. *Appl Phys Lett.* 2016;108:121903.

[11] Wei W, Mahdjoubi K, Brousseau C, Emile O. Generation of OAM waves with circular phase shifter and array of patch antennas. *Electron Lett.* 2015;51:442–443.

[12] Balanis CA. *Antenna Theory, Analysis and Design*. 3rd ed. New York: Wiley; 2005.

[13] Lalezari F, Massey CD. mm-wave microstrip antennas. *Microwave J.* 1987;30:87–96.

[14] Lee KF, Chen W. *Advances in Microstrip and Printed Antennas*. Wiley; 1997.

How to cite this article: Choi J-W, Oh S-S. Design of a circular array antenna for generating waves with orbital angular momentum. *Microw Opt Technol Lett.* 2017;59:2246–2249. https://doi.org/10.1002/mop.30713

Received: 20 February 2017

DOI: 10.1002/mop.30715

A dual-band polarization independent FSS having a transparent substrate for ISM and Wi-Fi shielding

Sultan Can[1] | **Kamil Yavuz Kapusuz**[2] | **Asım Egemen Yilmaz**[1]

[1] Department of Electrical and Electronics Engineering, Ankara University, Ankara, Turkey

[2] Department of Information Technology, Ghent University, Ghent, Belgium

Correspondence
Sultan Can, Department of Electrical Electronics Engineering, Ankara University, 50.Yil Kampusu, Golbasi, Ankara, 06830, Turkey.
Email: sultancan@ankara.edu.tr

Funding information
Ankara University Scientific Research Fund (BAP)—BAP, Grant/Award Number: 16B0443005.

Abstract

This paper presents a dual-band, polarization independent FSS for ISM and Wi-Fi shielding. The proposed structure has a band-stop characteristic for 2.5 and 5.1 GHz with a fractional bandwidth of 42% and 7%, respectively. The substrate of the FSS is a transparent material having a permittivity value of 2.77 and a thickness value of 1.48 mm, which provides band-pass characteristics for visible spectrum. The design, fabrication, and measurement of FSS were conducted for TM and TE polarizations; and satisfactory agreement was obtained.

KEYWORDS

dual-band, frequency selective surface, polarization independent, visible spectrum

1 | INTRODUCTION

Over many years, studies on electromagnetic pollution received a great attention from the research community due to the high degree of growth in mobile technology which ultimately increased the electromagnetic radiation. Interference caused by electromagnetic pollution is a serious threat to functioning of medical, military, and many other critical equipment.[1] Many studies have reported that GSM, ISM and Wi-Fi bands are the major contributors for the total electromagnetic interference.[2–4] Therefore, there exists a great demand for electromagnetic shielding to combat the effects of the radiated emission from the pollution.

Frequency selective surfaces (FSSs) are usually composed of periodically arranged metallic or slot patterns that function as band-stop or band-pass filters, respectively.[5,6] Various studies have been found to shield the GSM, ISM, and Wi-Fi signals, which interfere with the operation of the electronic equipment and FSSs have been attractive for such applications in spatial microwave and optical filters.

In this paper, a dual-band polarization independent FSS with band stop characteristic is proposed to suppress the electromagnetic radiations. With the proposed structure, which is designed on a transparent material, an indoor shield for both 2.5 and 5.1 GHz, have been realized. It acts as a band-stop filter for the two operating bands in microwave region and as a band-pass filter for visible region. In addition, the proposed FSS is polarization-independent and angular-insensitive. For sake of demonstration, a prototype of the FSS was fabricated and measured. The measurement results agree with the simulations having a high accuracy.

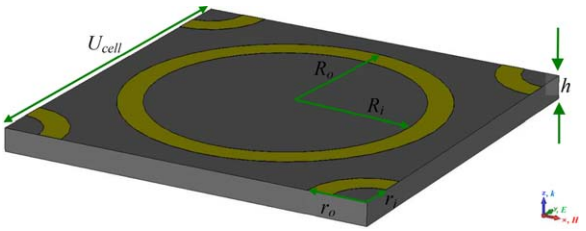

FIGURE 1 Geometry of the dual-band FSS. [Color figure can be viewed at wileyonlinelibrary.com]

2 | A DUAL-BAND FSS DESIGN AND NUMERICAL RESULTS

The proposed dual-band FSS structure consists of one large annual ring and four identical quarter small annual rings on the corners. Inner and outer radii of the large annual ring are determined as R_i and R_o, respectively. Each small annual ring located at the corners has an inner radius of r_i and outer radius of r_o. The substrate is a nylon based material having a permittivity value of $\varepsilon_r = 2.77$ with a thickness value of $h_s = 1.48$ mm.[7] The conductor patterns are made of an aluminum layer having a thickness of $h_c = 0.035$ mm on a substrate having a side length value of $U_{cell} = 5$ cm. Throughout the simulation periodic boundary conditions are imposed around the unit cell, and the excitation is as shown in Figure 1.

The increment of the R_i which cause a narrower conductor line for the larger annual ring, does not affect the upper frequency; however, it has an impact on lower frequency (see Figure 2A) as expected. The inductance of circular loop can be defined as in the following equation;

$$L_{loop} \approx \mu_0\mu_r\left(\frac{2\times R_o}{2}\right).\left(\ln\left(\frac{8\times(2\times R_0)}{R_o - R_i}\right)-2\right) \quad (1)$$

As mentioned in the equation, the decrement in the conductor width (R_o–R_i) cause an increment in the inductance value, which causes a decrement in S_{21} resonance regarding the relation $f_r = 1/\sqrt{L_{total}C_{total}}$. The relation is similar for the small annual ring inner radius r_i, as well (see Figure 2B). The increment of r_i causes a decrement in conductor width of the small annual ring so the S_{21} resonance of the upper frequency decreases as expected. The change in the inner radius values of small and large annual rings allow the adjustability of the upper and lower S_{21} resonances, respectively. Although this change provides a mean to adjust each individual frequency, changing the outer radius is quite complicated since the change in the outer radius also changes the distance between the rings. Increasing the outer radius of the larger ring causes a decrement in both upper and lower frequency. The distance

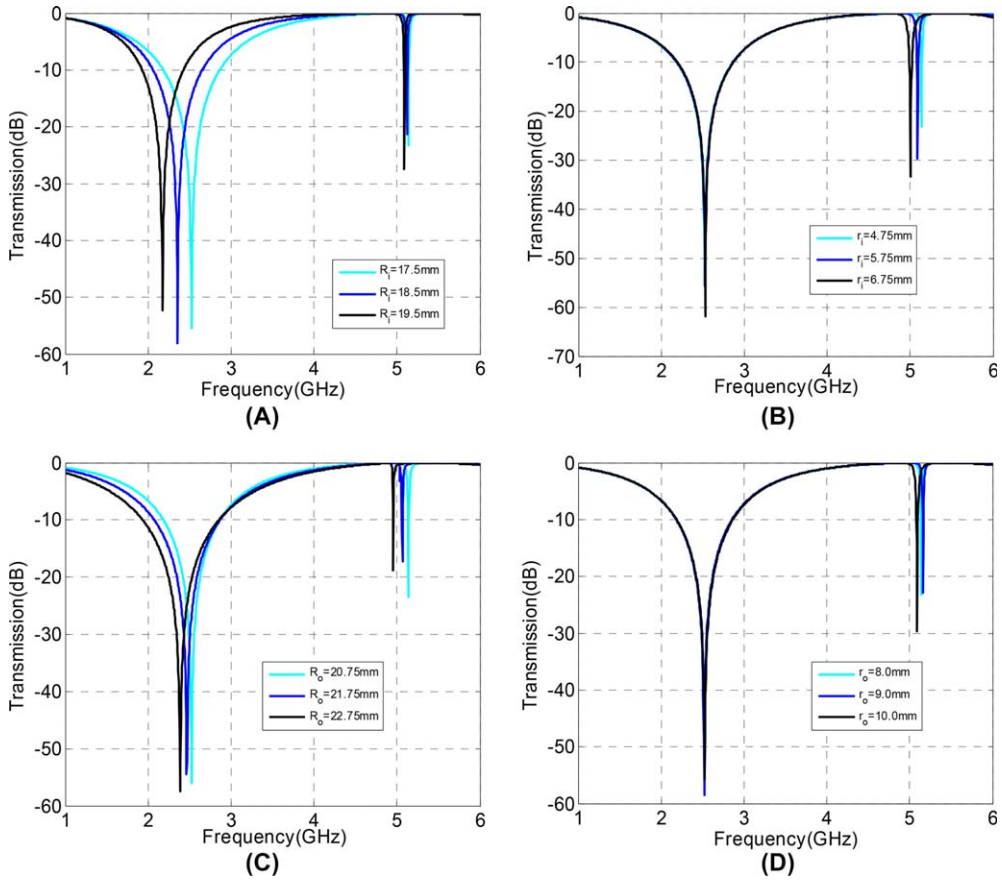

FIGURE 2 Transmission of proposed FSS under normal incidence as (A) R_i, (B) r_i, (C) R_o, and (D) r_o varies. [Color figure can be viewed at wileyonlinelibrary.com]

between the rings gets closer; this reduces the mutual capacitance value, which contributes the total capacitance value. Besides, due to the increment of R_o the self-inductance increases so that both frequency values decreases (see Figure 2C). Although increasing the r_i has the same effect in terms of mutual capacitance value, self-inductance value of the small ring has a small impact on upper frequency which we can claim to be quite negligible. Therefore, the increment of r_i causes a decrement in both S_{21} resonances.

The simulated results at normal incidence for both TE and TM polarizations are depicted in Figure 3. Obviously, the transmission coefficients are nearly constant for both polarizations because of the rotational symmetry in *x*-*y* plane. The figure sufficiently demonstrates that transmission performance of FSS are stable and insensitive for different angles.

The small annual ring, which contributes to higher frequency, causes more surface current as seen in Figure 4A for TE mode. For the upper frequency for again at TE mode the

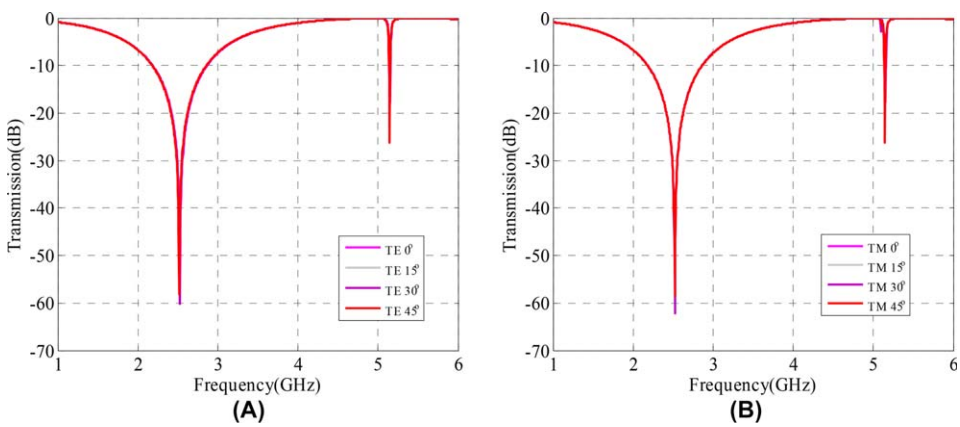

FIGURE 3 Transmission of proposed FSS for (A) TE and (B) TM polarizations with different normal incident angles. [Color figure can be viewed at wileyonlinelibrary.com]

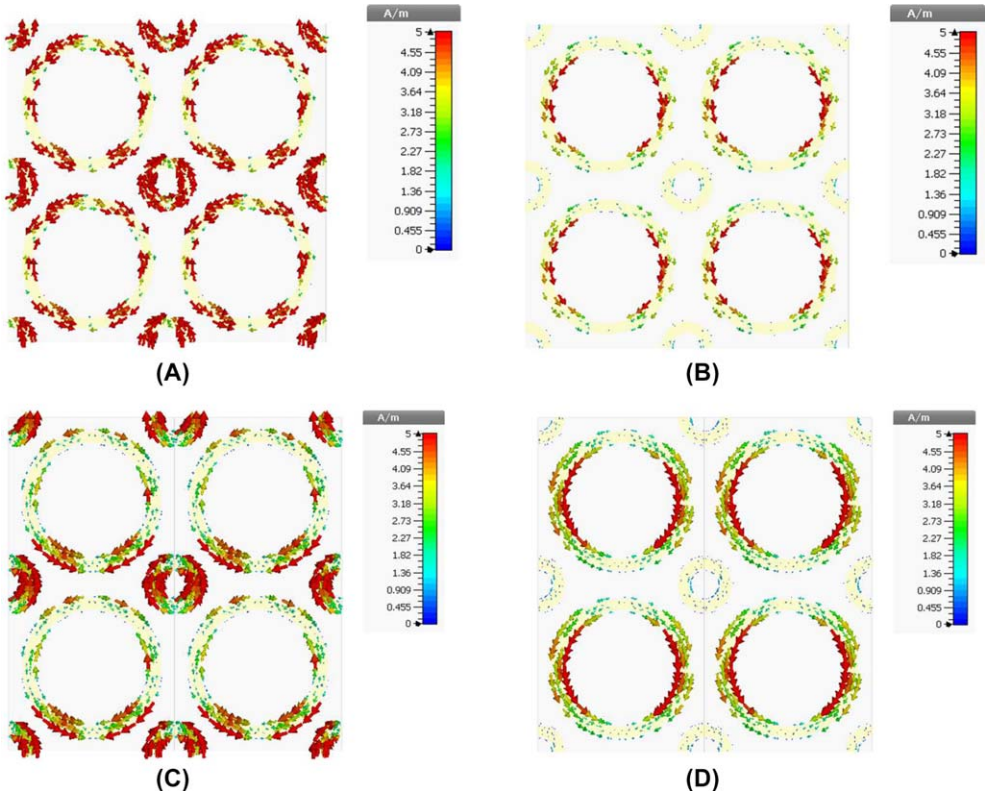

FIGURE 4 Current distribution on the proposed FSS (A) TE mode at $f = 5.1$ GHz, (B) TE mode at $f = 2.5$ GHz, (C) TM mode at $f = 5.1$ GHz, (D) TM mode at $f = 2.5$ GHz. [Color figure can be viewed at wileyonlinelibrary.com]

intensity of the surface current is more at the larger annual rings as in Figure 4B. As expected, since the structure is polarization independent, the upper and lower frequency values observed at the same frequency band and the intensity of the surface current has similar characteristics when compared to the TM mode (see Figure 3C,D).

3 | EXPERIMENTAL RESULTS

The unit cell periodic boundary condition is used for simulating the sample at the first step with an array of infinite unit cells in two dimensions. In order to mimic the array with better accuracy, an array of 10 × 10 elements is simulated and the sample is manufactured due to these results. The fabricated prototype is constructed to be a 10 × 10 array as seen in Figure 5.

The measurement set up is presented in Figure 6. The 10 × 10 array is located in the midpoint of the measurement set up, between two Rohde & Schwarz HF907 double-ridged waveguide horn antennas (800 MHz to 18 GHz) which are

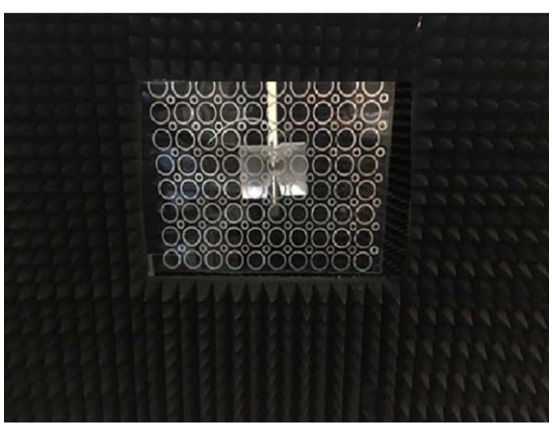

FIGURE 5 Fabricated dual-band FSS. [Color figure can be viewed at wileyonlinelibrary.com]

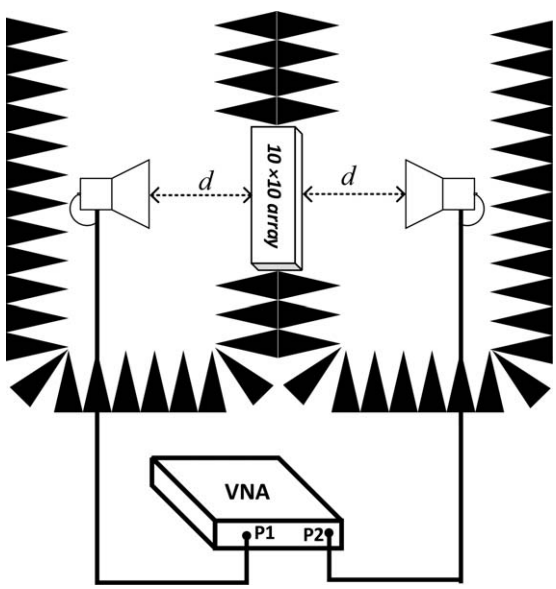

FIGURE 6 Measurement set-up of the dual-band FSS

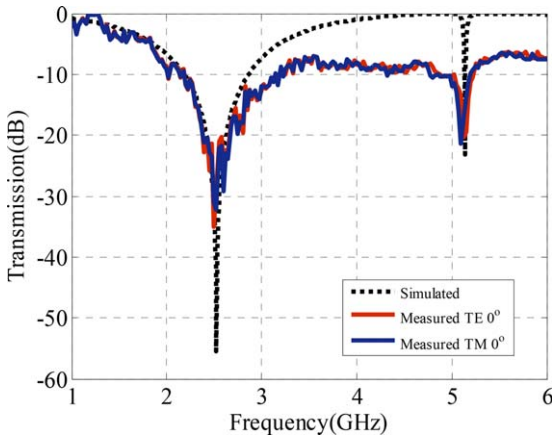

FIGURE 7 Simulated and measured transmissions at normal incident for TE and TM polarizations. [Color figure can be viewed at wileyonlinelibrary.com]

130 cm away from the sample. In order to reduce the interference and isolate the environment, TDK absorbers are placed to surround the measurement set up. Rohde & Schwarz ZVL13 Vector Network Analyzer, which is capable of measuring a frequency interval of 9 kHz to 13.6 GHz, is used throughout the measurements. In order to satisfy the proper angle values of the array and for preventing any bending of the structure, a slab layer of Polystyrene EPS Foam is used which has a dimension of 60 cm × 60 cm on the backside of the sample. It should be noted that the electrical properties of foam are similar to the free space so that we consider that the slab approximately satisfies $\varepsilon_r \approx 1$ and $\mu_r \approx 1$. However, due to the small difference of the relative permittivity and permeability values, small shifts in the frequency values are observed as expected.

The reasons for the small differences between the simulation and measurement (Figure 7) can be explained as follows. First, the results obtained by simulations are conducted under the assumption that there is an infinite size of array; however, in measurement it is an array of 10 by 10 elements. We can claim that the number of the array size has an impact of measurements and it contributes to the error in the measurement. The manufacturing error of the array and using Polystyrene EPS Foam layer may also cause the variety in the frequency and bandwidth differences in measurements.

4 | CONCLUSION

In this study, a dual-band FSS proposed for ISM and Wi-Fi shielding applications. FSS can filter the frequency band at 2.5 GHz having a bandwidth of 1.05 and 5.1 GHz having a bandwidth of 0.357 GHz. At the two rejection frequencies, 2.5 and 5.1 GHz the transmission below −30 and −20 dB have achieved. The proposed FSS achieve to have the same response for both TE and TM polarization, so that it can be used for both polarization without any necessity of modification of the structure. To the authors' best knowledge, the proposed polarization-independent FSS is also different from the ones in the literature since:

- it demonstrates polarization independency for each dual-band characteristics; and
- it has a transparent substrate to achieve band-pass characteristic for the visible band at the same time.

In addition to the structure's band-pass characteristics for the visible band, it has band-stop characteristics for 2.5 and 5.1 GHz frequencies. The proposed structure is manufactured to have 10 × 10 array; and satisfactory agreement between the measurements and the simulations are obtained.

ACKNOWLEDGMENTS

This work is supported by the Ankara University Scientific Research Fund (BAP)—BAP Grant No.: 16B0443005. Sultan Can also acknowledges TUBITAK for supporting her stay at Boston University during her Ph.D. studies through Program 2214A.

REFERENCES

[1] Pachón-García FT, Fernández-Ortiz K, PaniaguaSánchez JM. Assessment of Wi-Fi radiation in indoor environments characterizing the time & space-varying electromagnetic fields, Measurement. *J Int Measure Confederat.* 2015;63:309–321.

[2] Yan M, Qu S, Wang J, et al. A miniaturized dual-band FSS with stable resonance frequencies of 2.4 GHz/5 GHz for WLAN applications. *IEEE Antenna Wireless Propagat Lett.* 2014;13:895–898.

[3] Kiermeier W, Biebl E. New dual-band frequency selective surfaces for GSM frequency shielding. European Microwave Conference; 2007, 222–225; Munich.

[4] Sivasamy R, Murugasamy L, Kanagasabai M, Sundarsingh EF, Gulam Nabi Alsath M. A low-profile paper substrate-based dual-band FSS for GSM shielding. *IEEE Transact Electromagnet Compatib.* 2016;58:611–614.

[5] Unal E, Gokcen A, Kutlu Y. Effective electromagnetic shielding. *IEEE Microwave Mag.* 2006;7:48–54.

[6] da Silva Segundo FCG, Campos ALPS, Braz EC. Wide band frequency selectıve surface for angular and polarization independent operation. *Microwave Opt Technol Lett.* 2015;57:216–219.

[7] Can S, Kapusuz KY, Yilmaz AE. Wideband transparent frequency selective surface. Electronics Letters, submitted.

How to cite this article: Can S, Kapusuz KY, Yilmaz AE. A dual-band polarization independent FSS having a transparent substrate for ISM and Wi-Fi shielding. *Microw Opt Technol Lett*. 2017;59:2249–2253. https://doi.org/10.1002/mop.30715